Physics-informed Machine Learning for Predicting Fatigue Damage of Wire Bonds in Power Electronic Modules

Stoyan Stoyanov [1], Tim Tilford [1], Xiaotian Zhang [2], Yihua Hu [3], Xingyu Yang [4], Yaochun Shen [4]
[1] School of Computing and Mathematical Sciences, University of Greenwich, London, UK
[2] Department of Electronic Engineering, University of York, York, UK
[3] Engineering, Faculty of Natural, Mathematical & Engineering Sciences, King's College London, London, UK
[4] Department of Electrical Engineering and Electronics, University of Liverpool, Liverpool, UK
Email: s.stoyanov@gre.ac.uk

Abstract

This paper details a novel physics-informed data-driven approach for developing computationally fast metamodels for predicting fatigue damage and its spatial distribution at common failure sites of power electronic components. The proposed metamodels aim to serve the end-users of these power components by allowing an informative model-based assessment of the thermal fatigue damage in the assembly materials due to different application-specific, qualification and user-defined load conditions, removing current requirements for comprehensive device characterisations and deploying complex finite element (FE) models. The proposed methodology is demonstrated with two different metamodel structures, a multi-quadratic function, and a neural network, for the problem of predicting the thermal fatigue damage due to temperature cycling loads in the wire bonds of an IGBT power electronic module (PEM). The results confirmed that the proposed approach and the modelling technology can offer FE-matching accuracy and capability to map highly nonlinear spatial distributions of the damage parameter over local sub-domains associated with material fatigue degradation and failure due to material/interfacial cracking.

1. Introduction

Assuring and assessing the reliability performance of power electronic modules (PEMs) deployed in different applications remains a key challenge for the industry [1-3]. Power components based on current packaging architectures are most susceptible to thermally induced fatigue damage of their wire bonds and the die attachment layer. While many studies contributed to the reliability modelling of PEMs [4-8], the informed deployment of these modules in different applications remains a challenge for the end-users. Driven by considerations for protecting intellectual property (IP), data on internal design and dimensions of power components and their bill of materials are not included in manufacturers' technical datasheets and thus are not readily available. To assure the required reliability of PEMs under application-specific load conditions, the end-users must engage in time-consuming and costly activities to characterise the component and to evaluate its reliability performance through modelling and/or physical testing.

Finite element (FE) modelling, coupled with lifetime prediction methodologies and models, offers a robust solution for this problem by predicting damage metrics for the expected failure modes, for example, the studies reported in [5-8]. Lifetime prediction methodologies for PEM have been also extensively developed, with much of the effort on establishing accurate models predicting the wire bonds lifetime under accelerated active and passive temperature cycling conditions that qualify the device for the respective application load. Most commonly, lifetime models such as Cofin-Manson and Paris laws require damage parameter values that are semi-empirically correlated to the cycles to failure. For the failure of wire bonds in PEMs, a damage metric is most often obtained with FE simulation, and commonly chosen as the plastic strain range per cycle. This lifetime modelling approach has been demonstrated extensively, and in many studies [6,9]. However, developing and using such FE-based computational models to predict damage, and then lifetime, is a complex task that requires characterisation data, specialist skills, computing hardware, and advanced simulation software tools, all of which are not available to many end-users.

In this work, the authors aim to address the above position through a methodology for developing fast and user-friendly damage prediction models that take advantage of the combined deployment of metamodeling and machine learning (ML) using physics-informed damage data, where the focus is on the realisation of spatial mappings of results through a geometric abstraction of the failure site. The metamodels protect the manufacturer's intellectual property by not disclosing and not requiring any information about the packaging design, the internal component layout and topology, and the bill of materials. At the same time, they can be deployed by end-users of power devices with ease, to allow assessing the damage under user-defined application loads and visualise the damage distribution, allowing for the informed deployment of power electronics components across different applications through a better understanding of their reliability performance under respective load conditions.

2. Methodology

The main attributes of the proposed methodology are the complete automation of all steps that require computation and the synthetic generation of physics-informed datasets required for the meta-modelling part of the approach. For a given PEM structure, a fully scripted high-fidelity FE model generation (parametric model) and design-of-simulations runs are carried out first. The models enable assessing the damage level at anticipated failure sites (e.g. in wire bonds, solder attachment, etc.) as a

function of user-defined cyclic loads, but other model input parameters that capture design or manufacturing variations can also be included. As with the traditional Response Surface modelling approach, the proposed methodology utilises several high-fidelity analyses in the thermal load design space but uses a robust multi-quadratic (MQ) metamodel structure and a Neural Network to model the load-damage relationships in the spatial domain of the failure site. Underpinned by physics-of-failure data for the PEM assembly materials' degradation or damage, and locational damage distribution data informed by the FEA analysis, these fast models are capable of providing predictions not only for a characteristic damage value of the respective failure mode (e.g. wire bond cracking and wire liftoff) but a much more detailed prediction for the spatial distribution of the damage parameter (using spatial abstraction of the true failure site's geometry). The latter is a very important attribute of the proposed approach as it enables a robust deployment of different lifetime models in the public domain that may have different definitions of the required lifetime model input value of the damage characteristic, which is often obtained through a location-dependent or a spatial subdomain-dependent calculation using the damage parameter predictions at the failure site.

The methodology steps are visually outlined with the block diagram given in Fig. 1 and are also described in Table 1.

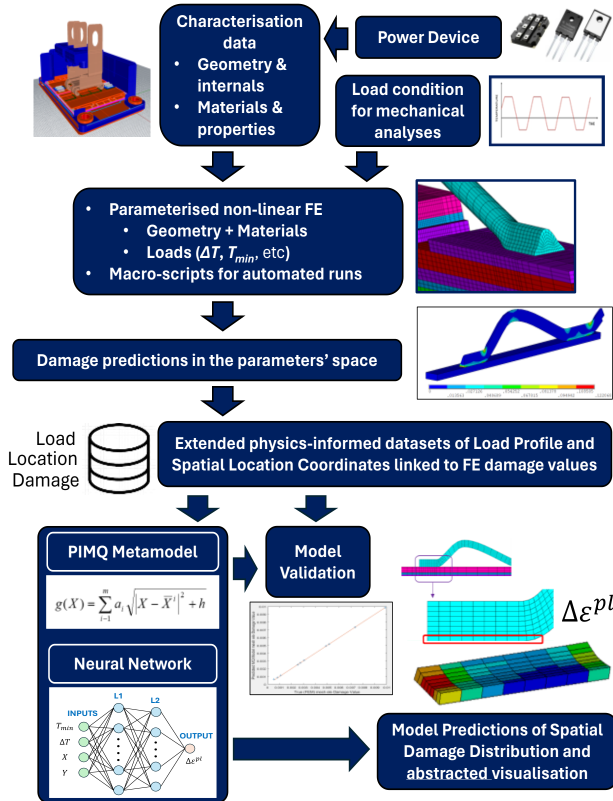

Figure 1: Methodology for physics-informed dataset generation, damage predictions and MQ and Neural Network metamodel development.

While in this study the methodology formulation, the demonstration and the metamodel validation focus on the realisation of the spatial damage distribution prediction capability of the metamodels, the methodological approach can be extended to the temporal domain too by defining and constructing a higher-dimension multi-variate MQ or Neural Network (NN) model structures.

Table 1. Methodological steps of the physics-informed metamodeling approach.

Step	Description
1	***Component Charatresiation Data***. If the metamodeling methodology is carried out by the manufacturer, to deliver metamodels to the end-user, without disclosing intellectual property, the component characterisation data will be readily available. Otherwise, the power device of interest must be fully characterised in terms of geometric data and materials.
2	***Loading Conditions Data***. The loading condition such as temperature cycling is parameterised. These load parameters are also the metamodel input parameters. Other parameters can be considered without any limitation.
3	***FE Modelling and Analyses Automation***. A parametric finite element model is developed using the characterisation data from Step 1, and FE simulation runs are scripted to allow the automation of all analyses for a defined set of data points in the parameter design space. An automated run of the FE simulations is executed. FE predictions for a defined damage parameter about a failure mode and mechanisms of the power module become available.
4	***Phytsics-Informed Datasets***. A spatial subdomain associated with the failure site of interest is defined. Extracting the FE prediction/data of interest from all analyses is scripted to enable the automation of this step. For the defined failure site spatial domain, mesh nodes/element's locations (coordinates) and element volumes are gathered along the respective FE predictions for the damage (nodal or element values).
6	***Extended Datasets and Data Labeling***. The physics-informed datasets in Step 5 are processed into the format of multi-variate data points with combined load and spatial location parameters. The data points are labelled with the associated damage value, as predicted by the FE simulation, for the respective load and spatial location.
7	***Metamodel Development***. A subset of the data (training dataset) is used to build a metamodel. Two model structures are suggested, MQ metamodel and Neural Network, both with excellent computational and predictive power characteristics. Realise the visualisation of metamodel results through a spatial domain abstraction of the failure site.
8	***Metamodel Validation***. Validation of models is performed using the balance of the data (the validation dataset), to assess model predictive power & accuracy.

3. Power Device and Thermo-mechanical Finite Element Model Development

The power electronic module that is investigated with the proposed damage prediction metamodeling methodology features a conventional IGBT packaging architecture with wire bond interconnections. Figure 2 shows a schematic of such a Power IGBT assembly. The actual Si chip (IGBT) is attached to a ceramic substrate, most commonly one of Alumina (Al_2O_3) or Aluminium Nitride (AlN). The substrate has copper metallization on both sides, in the form of thin layers with thickness typically around 300 μm, which are formed through direct thermal bonding (hence the reference to the metalized substrate as direct bond copper (DBC) substrate). The assembly of the chip and the DNC substrate is attached to the baseplate by soldering. The baseplate, typically Cu or AlSiN, provides the structural integrity for the entire package and acts as the interface with the heat sink which is a common thermal management solution.

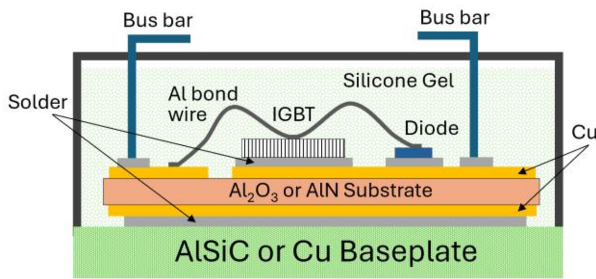

Figure 2: Schematic of a typical IGBT power module packaging architecture.

Further, non-schematic, details of the specific PEM that is modelled in this study are given in Fig. 3 (a). Here, the module's external plastic case is not visualised to reveal the internal construction of the assembly. In the set of wires, each wire has a bond and a stitch to the Si chip, and a bond at the other end to the copper trace pattern. In the modelling work, a 3D slice of the full module is captured, along the full length and through the thickness of the package, so that a single wire is fully represented.

Figure 3 (b) shows the 3D slice section as a CAD model and details the finite element mesh at the level of the wire bond. In addition, the materials that made the PEM are also annotated. The solder material providing the interconnection between the Si chip and the copper layer on the AlN substrate, and similarly between the DBC substrate and the AlSiC baseplate, is SnAg alloy. The thickness of the solder layers is 100 μm. In the FEA, the 96.5Sn3.5Ag solder is modelled as visco-plastic with the Anand constitutive law and model constants reported in [10,11]. Aluminium wires are Al-H11 alloy, with a diameter of 375 μm, and modelled with time-independent bilinear kinematic hardening material behaviour where the yield strength is temperature-dependent [12]. Due to the symmetry plane, only half of the 3D slice domain shown in Fig. 3(b) is used for the FE model and in the FE simulations.

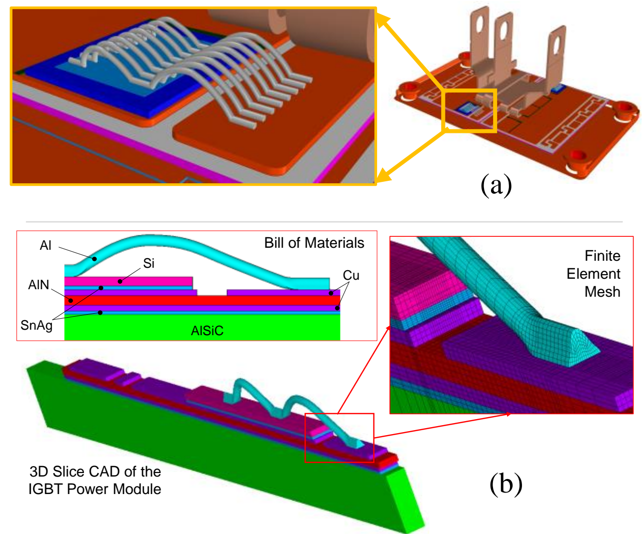

Figure 3: (a) Topology outline of the power electronic module architecture, with a close view of the IGBT chip and wire bonds, and (b) 3D CAD slice model of the device along the full length of the module, capturing a single wire, close view of the FE mesh density at the wire bond level, and annotation of the bill of materials.

Given the focus of this work, the PEM FE thermo-mechanical simulations are implemented in a fully automated manner, through ANSYS APDL scripting, where different thermal cycle load profiles are evaluated with the different simulation runs. The temperature cyclic load is defined with the low-temperature extreme value T_{min} and the temperature range ΔT of the cycle, where in this instance the ramp and dwell times are kept fixed. However, the ramp time/rate and dwell time can be also added to the load parameter design space to archive even further generalisation of the cycle load profile.

The FE model generation in the parameterised space of load-defining parameters is fully scripted using the ANSYS APDL command language and macro script functionality. This allows for the complete automation of simulation runs with different temperature cycle load parameters. For this problem, a single FEA simulation took about 50-65 minutes, determined by the load cycle duration that was simulated and was carried out using shared memory parallel with 16 processors of high-performance computing run on Intel(R) Xeon(R) processor workstation at 2.20 GHz, with 10 cores and 20 logical processors.

Figure 4 shows an example of FE simulation predictions for the plastic strain range due to one temperature cycle, $\Delta\varepsilon^{pl}$, in the wire bond domain next to the chip. The plastic strain range in that location is a commonly used indicator of material damage (damage parameter) that can be used in lifetime models to predict the wire liftoff failure due to bond cracking. Specifically, the interfacial mesh layer (here, with a thickness of 50 μm) is used to observe the damage distribution. This interfacial wire region is defined as the local spatial site for which the metamodels are developed.

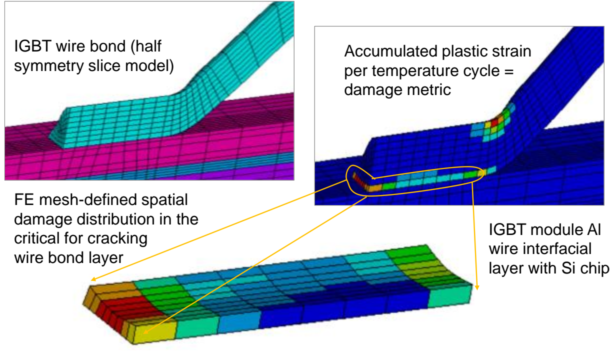

Figure 4: Example of FE simulation prediction of the plastic strain range (damage parameter) magnitude, $\Delta\varepsilon^{pl}$, and distribution in the Al wire bond (chip interface side). The interfacial layer where the crack is expected is defined as the local failure site of interest.

4. Physics-informed Meta-modelling of Damage Spatial Distribution

4.1 Datasets for Meta-modelling

The data required for metamodel development is generated with the parametrized thermo-mechanical finite element model and the automated run of 31 load-case simulations. Each analysis is a simulation of the PEM response to a particular passive temperature cyclic load that is defined with the minimum temperature and the magnitude of temperature excursion of the load, $(T_{min}, \Delta T)_i$, $i = 1, m$, where in this investigation m=31. Here, 21 of the load profiles are used to create the set of physics-informed damage data to be used to develop the metamodels (training data), and the remaining 10 load cases are used for validation of the metamodel accuracy against the respective FEA results. The cycling load profiles used to generate the training dataset are defined in a structured manner over a truncated T_{min} -ΔT design space to retain the physical feasibility of the cycle definition, as shown in Fig. 5. The following parameter levels are deployed:

- 6 levels of T_{min} in the range -55°C to 145°C
- 6 levels of ΔT, in the range 40°C to 240°C.

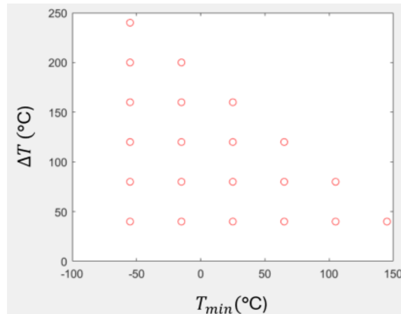

Figure 5: Temperature load-cycle cases analysed with FE simulations and used to establish the training dataset for metamodeling.

The load cases used to validate the developed metamodels are listed in Table 2.

Table 2. Temperature load-cycle cases used for metamodel validation.

		Load Case Ref. Number, #									
		1	2	3	4	5	6	7	8	9	10
Load	T_{min} (°C)	-35	-35	-35	-35	5	5	5	45	45	85
	ΔT (°C)	100	140	180	220	60	100	140	60	100	60

To demonstrate the concept of metamodels with the capability for mapping the spatial damage distribution, as it can be obtained with a full-order FE simulation, the local spatial domain of the Al wire bond at the interface with the chip is selected. This interfacial layer and how the damage parameter, $\Delta\varepsilon^{pl}$, is spatially distributed within are of prime interest for several reasons:

- This is the location of wire bond cracking due to thermal fatigue, leading to the wire lift-off failure.
- Lifetime models for the wire bond lift-off cycles to failure require the damage parameter values at this location, where the crack takes place.
- The special distribution information from a model is a critical requirement, to allow for the deployment of different approaches where the damage metric for the lifetime model may be formulated differently (for example volume weighted average over a region that may be different with different lifetime models).

The damage parameter spatial location values are associated with the FE mesh element centre locations for the mesh elements in the spatial domain of the failure site (i.e. the interfacial mesh layer shown in Fig. 4). Because the spatial domain demonstrated here is a planar layer at the wire bond to the chip interface with a single mesh division, only X and Y spatial coordinates need to be deployed. However, without any limitation, three-dimensional location definitions for more complex three-dimensional spatial domains of local failure sites within the global PEM domain can be defined similarly.

The mesh element of the wire-to-chip interfacial layer of interest is defined by a mesh grid with the size of 8×8, thus resulting in 64 spatial locations with coordinates (X_j, Y_j) , $j = 1,2, \dots ,64$.

The training dataset for building a metamodel is assembled as a combination of the load data points, $(T_{min}, \Delta T)_i$, $i = 1,,2, \dots ,21)$ and the location datapoints, (X_j, Y_j), $j = 1,2, \dots ,64$, resulting in 1,344 data points. Each data point in this extended dataset is a 4-dimensional vector normalized over the range [0,1]. Each of these points is labelled with the respective damage value $\Delta\varepsilon^{pl}$ at that location as obtained from the respective FE analysis at the location-matching mesh element. The damage values are also normalized over [0,1], based on the actual range

found with the training dataset. The same procedure is followed with the load-cycle cases set aside to generate the datasets for metamodel validation. The size of the validation dataset is 640 data points.

4.2 Multi-Quadratic (MQ) Metamodel

The multi-quadratic metamodel that is deployed in this work follows the surrogate modelling approach known as response surface methodology (RSM). RSM has become a popular tool in multi-disciplinary optimisation and conventionally uses polynomial functions to approximate a dataset of input points to known responses. A major issue with such polynomial metamodels is that they are not accurate in the case of non-linear response data. More complex model structures capable of interpolating the response data are required to address this challenge.

While metamodel structures based on Kriging and different radial basis interpolation functions have been demonstrated, highly non-linear data requires a model structure that in addition to the data interpolation feature allows for tuning the model accuracy away from the interpolation points.

In this study, the multi-quadratic (MQ) metamodel structure [13,14] is used, given with:

$$F_{MQ}(X) = \sum_{j=1}^{p} a_j \sqrt{|X - \bar{X}^j|^2 + h} \tag{1}$$

where $X \in R^n$ is the model input data point, i.e. the vector of n input model parameters, $\bar{X}^j \in R^n$ are the metamodel training points ($j = 1, \dots, p$) with known response values and h is the so-called shift parameter. The coefficients a_j in the multi-quadratic metamodel are computed by requiring the function in Eq. 1 to fit exactly the given set of finite element analysis response data $\left(\bar{X}^j,\ F_{MQ}(\bar{X}^j)\right)$ for the data points deployed in the model development ($j = 1, \dots, p$). This requirement results in solving a linear system of p equations with the coefficients in the multi-quadratic model a_j ($j = 1, \dots, p$) as unknowns.

A major advantage offered by the MQ method is its excellent ability to control the smoothness of the output parameter predictions through the model parameter h. This parameter has a major influence on the model accuracy. By altering the shift parameter value, the MQ accuracy can be improved dramatically.

The data points defined as the "training dataset" in section 4.1 are used to construct the MQ metamodel. At the training points, the MQ model predictions have zero error because of the interpolation attribute of the model structure. Hence, the accuracy of the model is judged by analysis of its predictive power using the data points in the validation dataset. The validation data has been also used to optimally tune the shift parameter h. The optimal value obtained for this problem and the datasets that were used is $h = 0.7$. The MATLAB programming environment is used to realise the required dataset processing and manipulation, the coding of the MQ model structure and solving the metamodel structure parameters.

Figure 6 shows the accuracy of the MQ metamodel, by plotting the actual FE simulation predictions vs. the metamodel predictions for the datapoints in the validation dataset. Both the MSE and the R-squared values show that the MQ offers exceptional accuracy for predicting the damage parameter value $\Delta\varepsilon^{pl}$ at the locations of interest and under varying load conditions. The predictive power of the model is even more impressive given the highly non-linear spatial distribution of the damage parameter at the wire bond interface region with the chip, as illustrated well with the example in Fig. 4.

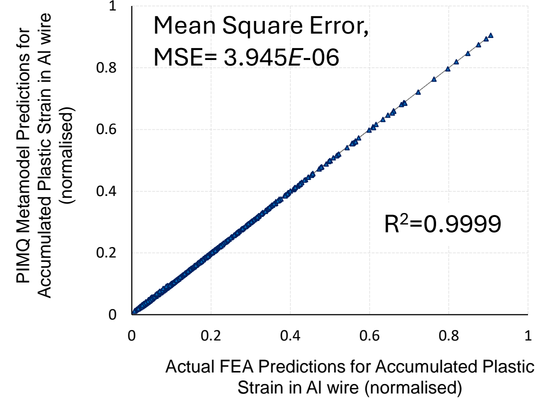

Figure 6: MQ predicted values vs. ground truth FEA values of the [0,1]-normalised plastic strain range per cycle values $\Delta\varepsilon^{pl}$ obtained for the validation dataset (640 points). Each data point in the validation dataset represents a cyclic thermal load condition (T_{min}, ΔT) and a planar (X,Y) spatial location of the wire bond to chip interface.

4.3 Neural Network (NN) Metamodel

The availability of labelled datasets also suits the deployment of machine learning algorithms in the task of creating regression-type predictive models. As an alternative to the MQ metamodeling approach, the training dataset is used to train a regression Neural Network model structure with four inputs, (T_{min}, $\Delta T, X, Y$), and a single output, $\Delta\varepsilon^{pl}$. The MATLAB scientific programming environment is used to realise the NN model development, by deploying a hyperparameter optimisation procedure during the training process. A fully connected model structure with 2 hidden layers and size (38, 35), and the rectified linear unit (ReLU) activation function for the fully connected layers of the neural network model, were found to minimise the loss function most effectively. The actual minimisation of the mean squared error (MSE), i.e. the loss function in the NN training process, was performed with the limited-memory Broyden-Fletcher-Goldfarb-Shanno quasi-Newton algorithm (L-BFGS) [15]. The model structure also deploys the standardized form of the predictor data, i.e. each numeric predictor variable is cantered and scaled by the corresponding variable mean and standard deviation given by the dataset parameter's values.

The accuracy of the NN model is detailed in Fig. 7. The actual FEA values of the damage parameter are predicted very well by the NN model. Although the MSE error of the

NN model for the validation dataset is about two times higher compared with the MSE of the MQ-metamodel, it remains extremely small, with the R-squared value close to 100%.

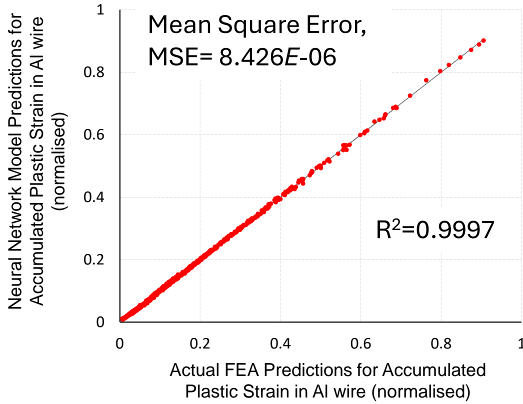

Figure 7: Neural Network predicted values vs. ground truth FEA values of the [0,1]-normalised plastic strain range per cycle values $\Delta\varepsilon^{pl}$ obtained for the validation dataset (640 points). Each data point in the validation dataset represents a cyclic thermal load condition (T_{min}, ΔT) and a planar (X,Y) spatial location of the wire bond to chip interface.

3. Results and Discussions

The model accuracy indicators detailed in the previous section suggest that both the physics-informed MQ metamodel and the NN model have excellent predictive power, matching very closely the actual FEA predictions for the parameter of interest ($\Delta\varepsilon^{pl}$). While here the focus is on the demonstration of the approach and hence only 64 spatial locations are included in the model, the $\Delta\varepsilon^{pl}$ values at these locations have very different magnitudes, yet such highly non-linear spatial distribution is accurately captured with the two investigated models. Even more, the approach is scalable, particularly in expanding the number of spatial locations for which the metamodel will provide predictions. This offers some interesting opportunities for reasonably detailed and informative mapping of physics-based parameter results in 3-dimensional subdomains of a physical system.

Figure 8 demonstrates the FE, MQ and NN model predictions for the $\Delta\varepsilon^{pl}$ at the failure site of interest, for the validation load case #6 (see Table 2, the load-cycle profile defined with $T_{min} = 5°\text{C}$ and $\Delta T = 100°\text{C}$). Here, a top view of the 3-dimensional layer, of the Al wire bond interface with the Si chip in the PEM, is visualised. The bottom contour plot is the FE results obtained from a non-linear transient finite element simulation using ANSYS APDL. The upper two plots in the figure are the MQ and NN model predictions where the spatial locations used have mapped the FE mesh resolution of this sub-domain. All three plots use the same legend scale to allow for the visual compassion of the results. The MQ model predictions match the FE contour plot scale bands across all 64 mesh locations, and the NN results are also nearly identical except at a few locations.

The ability to achieve such accuracy is important in the context of the rationale for carrying out this investigation. From a practical point of view, assessing the reliability performance of the PEM, e.g. wire bond failure, through model predictions of damage and/or using conventional fatigue lifetime models (Coffin-Manson, Paris, etc.) need only the results of the damage metric at the failure site only, not across the entire structural domain. Yet, with the FE approach a full-order FE model is needed of the entire structure to capture the material interactions, all input data for the CAD model, material properties and their constitutive laws, and a transient simulation of the cyclic load, to allow ultimately for a subset of results that are needed to become available for the damage/lifetime predictions.

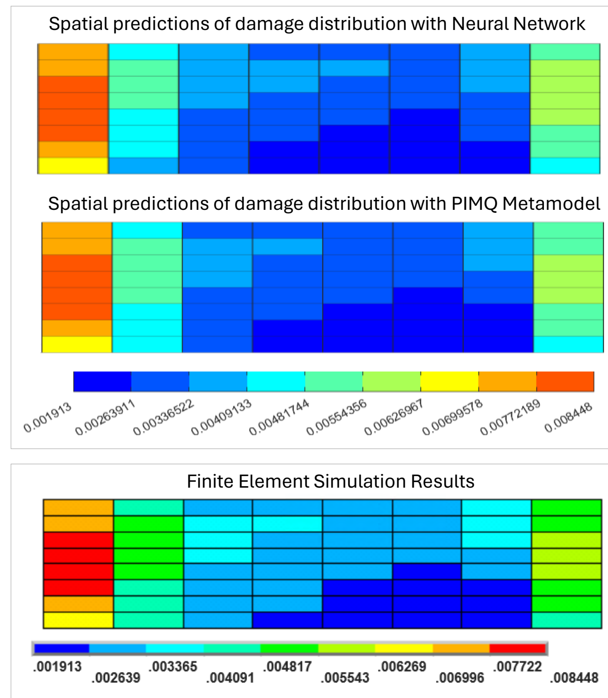

Figure 8: Damage map of Al wire bond at the interface with Si chip, defined with the mesh size and resolution of the FE model, predicted with (1) finite element analysis (bottom), (2) MQ metamodel (centre) and (3) Neural Network model (top). Results are for the validation case #6 defined with temperature cycle load $T_{min} = 5°\text{C}$ and $\Delta T = 100°\text{C}$.

With the proposed approach, such output is achieved with the same accuracy but comes with a great set of advantages. Firstly, once developed, the MQ/NN models allow for design exploration in the parameters space that excludes the spatial coordinate parameters. From a PEM end-user's point of view, this is predominantly the parametric space of the thermal load definition, allowing us to assess the PEM reliability performance under different load conditions as dictated by the different applications for which these modules are intended. With

the proposed modelling technology, end-users can do such evaluation without the need to fully characterise the PEM. Secondly, the MQ/NN models, once constructed, are real-time models – they provide predictions instantaneously. In contrast, non-linear FE simulation run times take minutes or hours.

While the MQ and NN metamodels provide predictions for the damage distribution in the failure site, many lifetime models correlate the cycles to failure with a characteristic damage value predicted for the failure site. In the case of FEA, commonly a volume-weighted average (VWA) of the damage parameter is obtained using mesh elements associated with the crack domain. In this instance, the wire bond interfacial domain with the chip for which the metamodels have been developed (as shown in Figures 4 and 8) is the volume for that calculation, and the damage parameter is the $\Delta\varepsilon^{pl}$:

$$\Delta\varepsilon_{ave}^{pl} = \frac{\sum_{i=1}^{m} \Delta\varepsilon^{pl}{}_{i} V_i}{\sum_{i=1}^{m} V_i} \quad (2)$$

where $\Delta\varepsilon_{ave}^{pl}$ is the VWA plastic strain range, V_i is the mesh element volume of element i, and the sums are over all elements (m) in the volume-weighted averaging domain.

Because the metamodel spatial predictions match the mesh resolution of the FE model, the calculation of the VWA damage representative metric (Eq. 2) for use with lifetime models can be also made based on MQ and NN model predictions for $\Delta\varepsilon^{pl}$. Such calculation would require the storage of volume data linked to the spatial locations of the domain.

Figure 9 shows a bar chart that compares the $\Delta\varepsilon_{ave}^{pl}$ values obtained with the FE, MQ and NN models for the ten validation load cases. Given the good accuracy of the MQ and NN metamodels at the individual locations that define the interfacial layer of the wire bond, as detailed in the previous section, the good agreement between these models in terms of the $\Delta\varepsilon_{ave}^{pl}$ prediction is also expected. The average absolute difference in the $\Delta\varepsilon_{ave}^{pl}$ strain value from the FE and PIMQ models is 3.5E-5, and in the case of the FE and the NN models that difference is 2.2E-5.

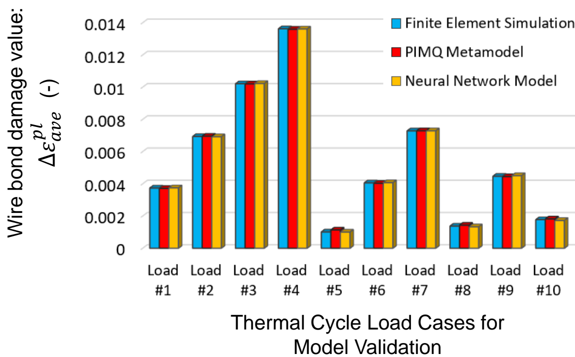

Figure 9: Wire bond VWA damage values $\Delta\varepsilon_{ave}^{pl}$ obtained by high-fidelity non-linear FEA, PIMQ metamodel and Neural Network model for the 10 different model validation load cases.

4. Conclusions

A novel approach for metamodel development using advanced interpolation methods and machine learning technology is formulated and demonstrated. While the methodology follows the well-established Response Surface Approach that is deployed in design optimisation studies, this work extends the concept beyond the prediction of a physical parameter. The metamodeling framework extends to the spatial domain and can equally handle in the same manner temporal predictions. It takes advantage of the capability of MQ and ML to handle large datasets with highly non-linear behaviour of the response data.

The advantage of the proposed metamodels is that no PEM data is required to run these models, and the runtime of analysis is only a fraction of the time that the FE simulation takes. The proposed models can be provided by PEM manufacturers along with PEM datasheets, to allow for the component IP protection while enabling the end-users to assess the reliability performance of the PEM under the loads and conditions of their application.

Acknowledgements

This work was supported by the Engineering and Physical Sciences Research Council (EPSRC), U.K., through project grant EP/R004390/1 and the linked grants EP/W006642/1, EP/W006405/1, and EP/W006308/1.

References

1. Wang, H., and Blaabjerg, F., "Power electronics reliability: state of the art and outlook," *IEEE Journal of Emerging and Selected Topics in Power Electronics*, Vol. 9, no. 6 (2021), pp. 6476-6493, doi: 10.1109/JESTPE.2020.3037161.
2. Yang, Y., Dorn-Gomba, L., Rodriguez, R., Mak, C., and Emadi, A., "Automotive power module packaging: current status and future trends," *IEEE Access*, Vol. 8 (2020), pp. 160126-160144, doi: 10.1109/ACCESS.2020.3019775.
3. Gonzalez, J.O., *et al.*, "Enabling high reliability power modules: A multidisciplinary task," *Proc. International Symposium on 3D Power Electronics Integration and Manufacturing*, Raleigh, NC, USA, 2016, pp. 1-5, doi: 10.1109/3DPEIM.2016.7570567.
4. Li, Q., *et al.*, "Review of the failure mechanism and methodologies of IGBT bonding wire," *IEEE Transactions on Components, Packaging and Manufacturing Technology*, Vol. 13, no. 7 (2023), pp. 1045-1057, doi: 10.1109/TCPMT.2023.3297224.
5. Huang, Q., Peng, C., Ellen, S.F.-M., Zhu, W., and Wang, L., "A Finite Element Analysis on the reliability of heavy bonding wire for high-power IGBT module," *IEEE Transactions on Components, Packaging and Manufacturing Technology*, Vol. 11, no. 2 (2021), pp. 212-221, doi: 10.1109/TCPMT.2020.3028386.
6. Rajaguru, P., Lu, H., and Bailey, C., "Time integration damage model for Sn3.5Ag solder interconnect in Power Electronic Module," *IEEE Transactions on*

Device and Materials Reliability, Vol. 19, no. 1 (2019), pp. 140-148, doi: 10.1109/TDMR.2019.2891949.
7. Dudek, R., *et al*., “Reliability modelling for different wire bonding technologies based on FEA and nano-indentation,” *Proc. 8th Electronics System-Integration Technology Conference*, Tønsberg, Norway, 2020, pp. 1-7, doi: 10.1109/ESTC48849.2020.9229761.
8. Shishido, N., Hayama, Y., Morooka, W., Hagihara, S., and Miyazaki, N., “Application of nonlinear fracture mechanics parameter to predicting wire-liftoff lifetime of Power Module at elevated temperatures,” *IEEE Journal of Emerging and Selected Topics in Power Electronics*, Vol. 7, no. 3 (2019), pp. 1604-1614, doi: 10.1109/JESTPE.2019.2914244.
9. [ref04] Grams, A., Prewitz, T., Wittler, O., Schmitz, S., Middendorf, A., and Lang, K.-D., “Modelling the lifetime of aluminum heavy wire bond joints with a crack propagation law,” *Proc. 15th EuroSimE Conference*, Ghent, Belgium, 2014, pp. 1-6, doi: 10.1109/EuroSimE.2014.6813828.
10. [ref01] Wang, G. Z., Cheng, Z. N., Becker, K., and Wilde, J., “Applying Anand model to represent the viscoplastic deformation behavior of solder alloys,” *ASME Journal of Electronic Packaging*, Vol. 123, No. 3 (2001), pp. 247-253, doi: 10.1115/1.1371781.
11. [ref02] Cheng, Z. N., Wang, G. Z., Chen, L., Wilde, J. and Becker, K., "Viscoplastic Anand model for solder alloys and its application", *Soldering & Surface Mount Technology*, Vol. 12, No. 2 (2000), pp. 31-36, doi: 1108/09540910010331428.
12. [ref03] Milke, E. and Mueller, T., “High temperature behaviour and reliability of Al-Ribbon for automotive applications,” *Proc. 2nd Electronics System-Integration Technology Conference*, Greenwich, UK, 2008, pp. 417-422, doi: 10.1109/ESTC.2008.4684384.
13. [ref05] Hardy, R. L., “Multiquadratic equations of topography and other irregular surfaces,” *Journal of Geophysical Research*, Vol. 76, Issue 8 (1971), pp. 1905-1915, doi: 10.1029/JB076i008p01905.
14. [ref06] Wang, B., “Parameter optimization in multiquadric response surface approximations,” *Structural and Multidisciplinary Optimization*, Vol. 26 (2004), pp. 219-223, doi: 10.1007/s00158-003-0341-4.
15. [ref07] Liu, D. C., and Jorge Nocedal, J., “On the limited memory BFGS method for large scale optimization,” *Mathematical Programming*, Vol. 45, No. 1 (1989), pp. 503-528, doi: 10.1007/BF01589116.